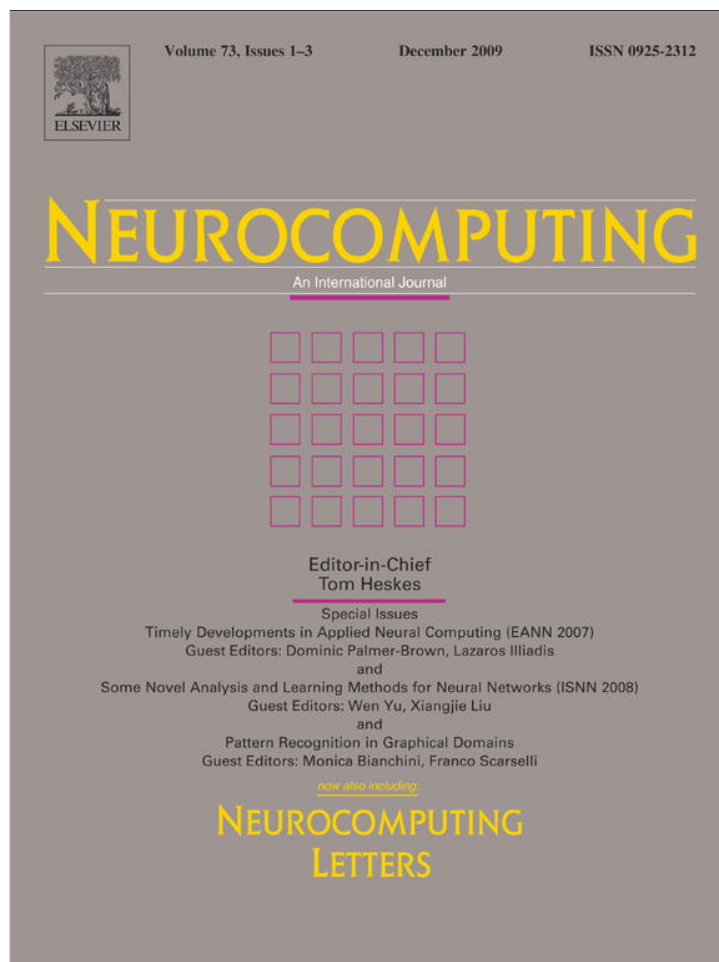


Provided for non-commercial research and education use.
Not for reproduction, distribution or commercial use.



This article appeared in a journal published by Elsevier. The attached copy is furnished to the author for internal non-commercial research and education use, including for instruction at the authors institution and sharing with colleagues.

Other uses, including reproduction and distribution, or selling or licensing copies, or posting to personal, institutional or third party websites are prohibited.

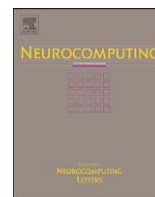
In most cases authors are permitted to post their version of the article (e.g. in Word or Tex form) to their personal website or institutional repository. Authors requiring further information regarding Elsevier's archiving and manuscript policies are encouraged to visit:

<http://www.elsevier.com/copyright>



Contents lists available at ScienceDirect

Neurocomputing

journal homepage: www.elsevier.com/locate/neucom

Transient responses of activity-dependent synapses to modulated pulse trains

Christian Mayr, Johannes Partzsch^{*}, Rene Schüffny

Chair for Parallel VLSI Systems and Neural Circuits, University of Technology Dresden, Germany

ARTICLE INFO

Available online 4 August 2009

Keywords:

Activity-dependent synapses
 Transient pulse transmission
 Modulated pulse train
 Synaptic response

ABSTRACT

Synapses exhibit complex filtering properties on short time scales with respect to their presynaptic pulse trains. In particular, the quantal model of neurotransmitter release has been shown to be highly selective for particular presynaptic pulse patterns. However, due to the iterative, pulse-based nature of the original equations describing the quantal model, such analysis has been relegated to heuristics and simulations. In contrast, we derive an explicit expression for the quantal model and apply it to analyzing the transmission of modulated pulse trains across a synapse. We show that for biologically realistic parameters, the quantal model favors periodically modulated pulse trains (such as bursting, chattering or stuttering) over non-modulated (i.e. regular) ones.

© 2009 Elsevier B.V. All rights reserved.

1. Introduction

The main computational function of artificial neural networks has traditionally been modelled as an adjustment of the coupling weight between neurons. In biological nets, this coupling weight is provided by synapses, where an incoming (presynaptic) pulse causes a release of neurotransmitters, which in turn generate a postsynaptic current (PSC) that charges the postsynaptic (i.e. receiving) neuron membrane [10]. The synaptic weight W (size of the PSC) can be modelled as a function of three different variables [10]:

$$W = f(n, p, q), \quad (1)$$

with n , p and q denoting the number of synaptic release sites, the neurotransmitter release probability and the release quantity, respectively. These variables represent structural characteristics of biological neural networks [2].

Mechanisms acting on the number of release sites n seem to be targeted at long-term learning, while plasticity of the neurotransmitter release probability p and release quantity q both act on timescales of 0.1–1 s and are therefore well suited for extracting temporal fine structure of presynaptic pulse trains [1,9]. Even for long-term learning, this short-term synaptic filtering may influence the type of learning carried out [6]. Thus,

dynamic synapses execute various crucial signal transformations, for a review, see [1].

The plasticity of q has been modelled in an influential work by Markram et al. [11]. They introduced a formulation of quantal neurotransmitter release based on a descriptive model of biological mechanisms and measurements (in the following referred to as *quantal model*). Over the intervening years, the quantal model has been extensively studied with respect to its information transmission properties in single synapses [1,12,13,7] or in populations [14]. It has also been combined with other synaptic plasticity mechanisms to investigate possible interrelations with long-term learning [6,1] or probabilistic release models [12]. The model has also been employed in a VLSI realization of 'selective attention' neural information processing [4]. Various state of the art neuroscience efforts still use the original model e.g. in studies of pain reception [6], the differing modes of memory retrieval [16] or in the continuing effort to fully characterize the model itself and its various processing characteristics [15,16,6]. However, most of this work has been carried out via simulations, probably caused by the iterative, pulse-based nature of the model, making a closed solution, i.e. some kind of transfer function, intractable. In this work, we show that for regular pulse rates, the model by Markram et al. can be expressed explicitly as an exponential decay function. Absolute time constants of this exponential decay are derived in the appendix, based on the original iterative time constants and the underlying pulse rate. We use this derivation in Section 2 to analyze the response of a dynamic synapse to frequency modulated pulse trains. These modulated pulse trains [12,13], i.e. comprised of regular shifts between high and low pulse rates [8], constitute an important component of the repertoire of neural information transmission at

^{*} Corresponding author.

E-mail addresses: mayr@iee.et.tu-dresden.de (C. Mayr), partzsch@iee.et.tu-dresden.de (J. Partzsch), schueffn@iee.et.tu-dresden.de (R. Schüffny).

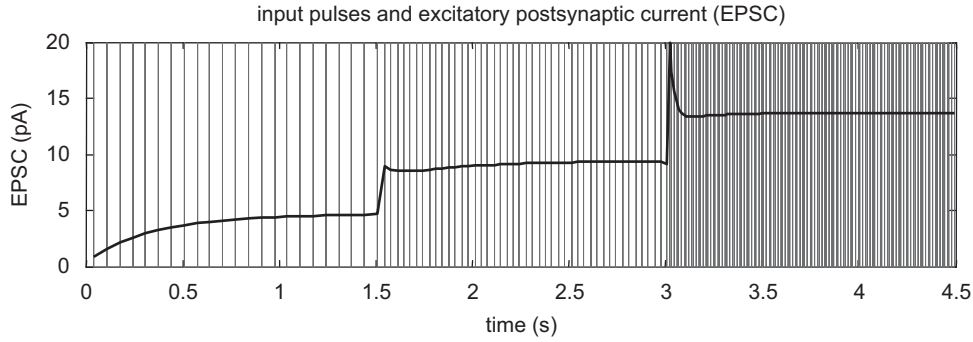


Fig. 1. Behavior of the quantal synaptic short-term adaption, protocol similar to [11, Fig. 4], but regular pulse rates instead of Poisson, frequency step after 1.5 and 3 s, pulse rates $15\text{ s}^{-1} \rightarrow 30\text{ s}^{-1} \rightarrow 80\text{ s}^{-1}$, the continuous curve denotes the resulting PSC (see footnote 1).

dynamic synapses. The veracity of the explicit expression and its application to modulated pulse trains is shown by comparison with simulations of the original quantal model. Also, comparison with similar work carried out via simulations in the literature [13,12] confirm the findings derived from our explicit solution.

2. Synaptic transmission of modulated pulse trains

2.1. Model of activity-dependent synapses

The model developed by Markram et al. [11] is governed by two parameters, utilization of synaptic efficacy u and available synaptic efficacy R . It is based on the assumption that there is a specific amount of neurotransmitter vesicles available to the synapse for transmission. Upon transmission of a presynaptic pulse, a certain fraction of these vesicles becomes instantaneously unavailable, decreasing R . Two mechanisms act to restore these vesicles. On the one hand, a constant recovery of R takes place. On the other hand, a facilitation process is activated that increases the utilization u with each presynaptic pulse. Facilitation thereby acts on a longer time scale than recovery, increasing synaptic response for intermediate pulse rates.

Both u and R are measured as fractions of maximum efficacy at pulse n of the pulse train. The iterative equations governing the evolution of u_n and R_n are as follows [11]:

$$u_{n+1} = u_n e^{-\Delta t_n / \tau_{\text{facil}}} + U \cdot (1 - u_n e^{-\Delta t_n / \tau_{\text{facil}}}), \quad (2)$$

$$R_{n+1} = R_n (1 - u_{n+1}) e^{-\Delta t_n / \tau_{\text{rec}}} + 1 - e^{-\Delta t_n / \tau_{\text{rec}}}, \quad (3)$$

with Δt_n denoting the time difference between pulses n and $(n + 1)$ of the pulse train. Utilization is increased (facilitated) with each pulse and recovers with a time constant τ_{facil} , while R recovers with τ_{rec} , dependent on the current utilization. The starting terms for (2) and (3) can be computed from the utilization U of a relaxed synapse (i.e. $\Delta t_0 \rightarrow \infty$) as $u_1 = U$ or $R_1 = 1 - U$, respectively [11]. The PSC caused by a presynaptic pulse is defined as the product of u_n and R_n , weighted with the absolute synaptic efficacy A (ratio of release quantity to resultant PSC):

$$\text{PSC}_n = A \cdot R_n \cdot u_n. \quad (4)$$

The effect of this adaption can best be described as transmission of transients, i.e. changes in the presynaptic pulse rate are transmitted with their full dynamic range to the postsynaptic neuron, but the response to steady-state input pulse rates diminishes (see Fig. 1). This seems to be a universal feature of biological neural nets, where novel stimuli receive increased responses compared to static ones [1,10].

For a steady-state signal, the above response can be thought of as a signal compression, so that the high dynamic range of e.g. sensory input is adapted to the limited range of the pulse response of a neuron [1]. The steady-state values that u and R settle to for a given pulse rate (Fig. 1¹) can be computed by equating u_n and u_{n+1} in (2) for a fixed pulse rate $\lambda = 1/\Delta t_n$ [11]:

$$u_c(\lambda) = \frac{U}{1 - (1 - U) \cdot e^{-1/\lambda \cdot \tau_{\text{facil}}}}. \quad (5)$$

Using this u_c and a similar equalization approach, the convergent R_c is derived as

$$R_c(\lambda) = \frac{1 - e^{-1/\lambda \cdot \tau_{\text{rec}}}}{1 - (1 - u_c(\lambda)) \cdot e^{-1/\lambda \cdot \tau_{\text{rec}}}}. \quad (6)$$

These equations confirm the finding of Fig. 1 that the steady-state PSC response for low pulse rates is amplified with a time constant τ_{facil} while the response for high pulse rates is attenuated with a time constant of τ_{rec} .

Fig. 2 shows the converged values with respect to the pulse rate λ . While synaptic efficacy R decreases with higher pulse rate, utilization u increases. This results in a relative PSC that increases to its maximum value at approx. 20 Hz and then slightly decreases, which is in agreement with [11,2]. Note that this is the response to a single presynaptic pulse; for a mean PSC response over a given time window, as it is the case in Fig. 1, this value has to be weighted by the pulse rate.

2.2. Analytical approach to synaptic transmission

For variable pulse rates, the attenuation of a stimulus should be limited so as not to lose important information about the stimulus resp. only attenuate static stimuli [10,14]. In the following, the PSC response of the Markram model to modulated stimuli is analyzed. A modulated pulse rate can be thought of as a sequence of bursts (see Fig. 3) and as such represents a generic model for various types of neural pulse signalling, where the information is encoded in the temporal fine structure of the pulse signal [8,12], or where bursts represent mechanisms in memory retrieval [16].

For the purpose of this study we approximate a natural spike train with interspaced bursts [13] (as shown in the upper graph of

¹ The parameters are identical to [11, Fig. 4], i.e. $\tau_{\text{facil}} = 530\text{ ms}$, $\tau_{\text{rec}} = 130\text{ ms}$, $A = 1540\text{ pA}$, $U = 0.03$. To derive a continuous PSC from the pulse-PSC of (4), pulses with a duration of 1.4 ms are weighted with the responses from (4), similar to the sum of PSCs as used in [13]. However, in contrast to [13], a moving average with a window of 100 ms is computed to obtain a time curve rather than a scalar figure of merit. The pulse duration is not explicitly mentioned in [11], but biological evidence [10] and the similarity of Fig. 1 with [11] support this value.

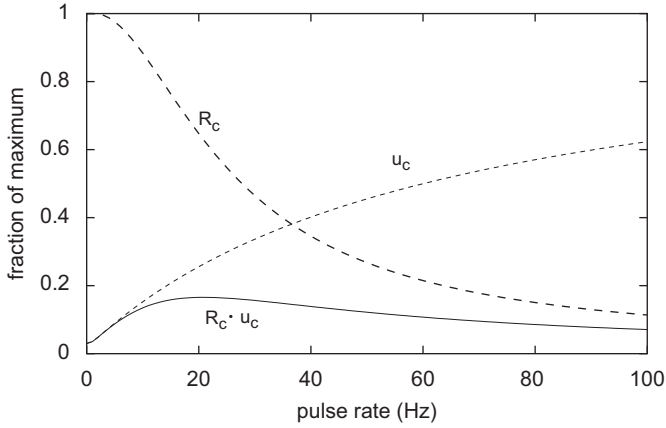


Fig. 2. Converged values of synapse model with respect to constant pulse rate.

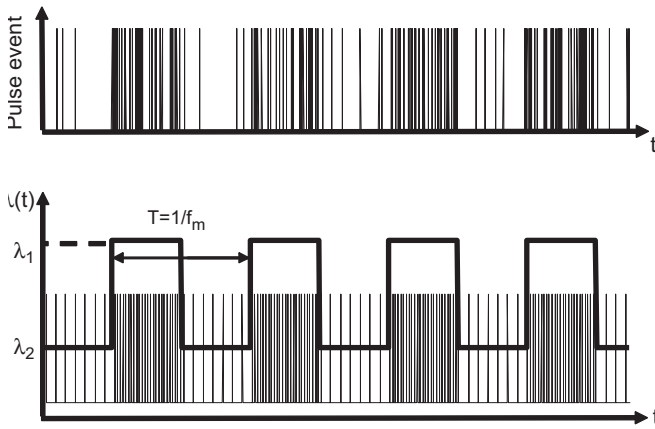


Fig. 3. From top to bottom: bursty spike train and regularized approximation with rectangular modulation between high pulse rate λ_1 and low pulse rate λ_2 with a modulation frequency of f_m .

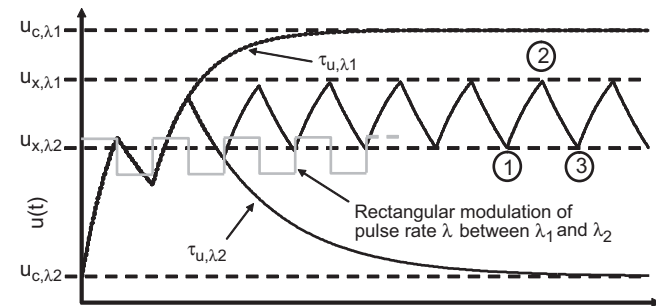


Fig. 4. Time course of $u(t)$ and its dependencies on modulation frequency f_m and convergence limits u_c for high and low pulse rates λ_1 and λ_2 , respectively. Presynaptic pulse rates of the dynamic synapse are modulated as depicted in Fig. 3.

Fig. 3) by a spike train with a rectangular modulation between two fixed pulse rates (lower part of Fig. 3).

As is shown in the appendix, in the case of such a piecewise constant pulse frequency, the convergence of $u(t)$ can be expressed by an exponential decay with a new absolute time constant $\tau_{u,\lambda}$ that is not only related to the original iterative time constant but also to the underlying pulse frequency. Fig. 4 qualitatively shows the time course of $u(t)$ for such a modulated stimulus. The value of $u(t)$ oscillates inside a fixed amplitude interval that depends on the modulation frequency f_m , on the convergence limits u_c for low and high pulse rates and on

the new absolute time constants τ_{u,λ_1} and τ_{u,λ_2} (see (20) in the appendix).

For the derivation of the PSC's modulation dependency, we start with the explicit expression of (2) as derived in the appendix. Dependent on the sign of the term $(u_0 - u_c)$, this equation describes one increasing or decreasing part of the time course, respectively:

$$u(t) = (u_0 - u_c)e^{-t/\tau_{u,\lambda}} + u_c. \quad (7)$$

For evaluating the integral over the average PSC, the initial values for each cycle must be calculated. These are generally not the limits of convergence, but intermediate values, as can be seen from Fig. 4. Their calculation will be shown exemplarily for u_{x,λ_2} in the following. Our approach is based on the observation, that the value of $u(t)$ at points 1 and 3 in Fig. 4 is the same in a steady state. Following the time course of $u(t)$ beginning at point 1 (assuming $t = 0$ there) yields:

$$u(t) = (u_{x,\lambda_2} - u_{c,\lambda_1})e^{-t/\tau_{u,\lambda_1}} + u_{c,\lambda_1} \rightarrow u\left(\frac{1}{2f_m}\right) = (u_{x,\lambda_2} - u_{c,\lambda_1})e^{-1/(2f_m\tau_{u,\lambda_1})} + u_{c,\lambda_1}, \quad (8)$$

with the second equation determining the value of $u(t)$ at the end of the high-rate interval. An analogous relation for the low-rate interval, i.e. the time course from point 2 to 3, results in

$$u\left(\frac{1}{f_m}\right) = u_{x,\lambda_2} = \left[u\left(\frac{1}{2f_m}\right) - u_{c,\lambda_2} \right] e^{-1/(2f_m\tau_{u,\lambda_2})} + u_{c,\lambda_2}. \quad (9)$$

Evaluating (8) and (9) leads to the following expression for u_{x,λ_2} :

$$u_{x,\lambda_2} = \frac{1}{1 - e^{-(\tau_{u,\lambda_1} + \tau_{u,\lambda_2})/(2f_m\tau_{u,\lambda_1}\tau_{u,\lambda_2})}} \left[u_{c,\lambda_1} e^{-1/(2f_m\tau_{u,\lambda_1})} (1 - e^{-1/(2f_m\tau_{u,\lambda_1})}) + u_{c,\lambda_2} (1 - e^{-1/(2f_m\tau_{u,\lambda_2})}) \right] \quad (10)$$

Results for u_{x,λ_1} , R_{x,λ_1} and R_{x,λ_2} can be derived with similar approaches.

Now, the mean synaptic release quantity \overline{UR} can be calculated. This is done by integrating the product $u(t) \cdot R(t)$ and normalizing the result with the integration interval. For the high-rate interval, i.e. the time course between points 1 and 2, the following holds:

$$\overline{UR}_{12} = 2f_m \cdot \int_0^{1/2f_m} [(u_{x,\lambda_2} - u_{c,\lambda_1})e^{-t/\tau_{u,\lambda_1}} + u_{c,\lambda_1}] \cdot [(R_{x,\lambda_2} - R_{c,\lambda_1})e^{-t/\tau_{R,\lambda_1}} + R_{c,\lambda_1}] dt. \quad (11)$$

Evaluating this integral results in

$$\overline{UR}_{12} = 2f_m \left[(u_{x,\lambda_2} - u_{c,\lambda_1})(R_{x,\lambda_2} - R_{c,\lambda_1}) \cdot \frac{\tau_{u,\lambda_1}\tau_{R,\lambda_1}}{\tau_{u,\lambda_1} + \tau_{R,\lambda_1}} \times (1 - e^{-(\tau_{u,\lambda_1} + \tau_{R,\lambda_1})/(2f_m\tau_{u,\lambda_1}\tau_{R,\lambda_1})}) + (u_{x,\lambda_2} - u_{c,\lambda_1})\tau_{u,\lambda_1}R_{c,\lambda_1}(1 - e^{-1/(2f_m\tau_{u,\lambda_1})}) + (R_{x,\lambda_2} - R_{c,\lambda_1})\tau_{R,\lambda_1}u_{c,\lambda_1}(1 - e^{-1/(2f_m\tau_{R,\lambda_1})}) + \frac{u_{c,\lambda_1}R_{c,\lambda_1}}{2f_m} \right]. \quad (12)$$

Integrating over the low-rate interval, i.e. the time course between points 2 and 3, in the same way yields the corresponding value \overline{UR}_{23} .

As mentioned together with Fig. 1, these mean values must be weighted by the number of pulses that occurred in the corresponding time interval. This can be done by using the ratio between the total time any pulse was active and the time interval:

$$\overline{PSC}_{xy} = A \cdot \frac{T_{\text{pulse}} N_{\text{pulse},x}}{T_{\text{norm}}} \cdot \overline{UR}_{xy} = A \cdot \frac{T_{\text{pulse}} (\lambda_x T_{\text{norm}})}{T_{\text{norm}}} \cdot \overline{UR}_{xy}. \quad (13)$$

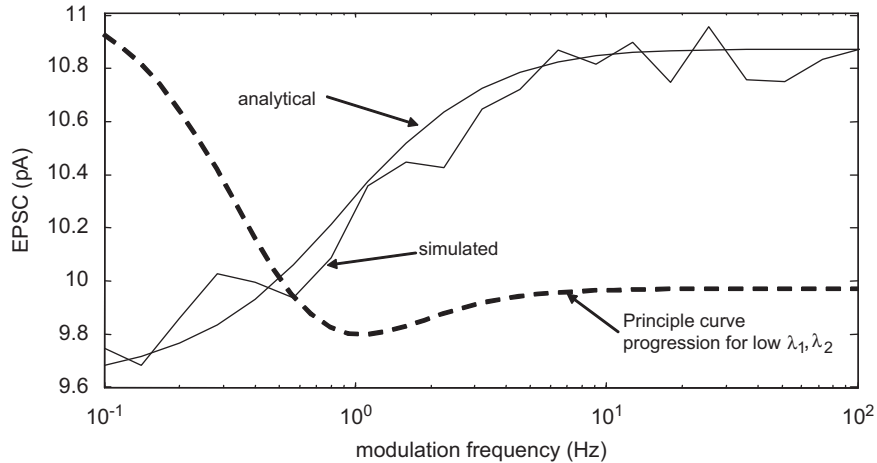


Fig. 5. Comparison of analytical and simulated PSC for $\lambda_1 = 130 \text{ s}^{-1}$ and $\lambda_2 = 6 \text{ s}^{-1}$. The simulated curve is an average over 30 repetitions. A rate-weighted average was used for calculating the mean PSC values shown in the figure. Additionally, the qualitative course of frequency dependence for $\lambda_1 = 70 \text{ s}^{-1}$ and $\lambda_2 = 2 \text{ s}^{-1}$ is also shown (dashed line, positive offset).

For both the high-rate and low-rate intervals, $T_{\text{norm}} = 1/2f_m$. Using the corresponding constant pulse rate, N_{pulse} can be calculated for each interval as $N_{\text{pulse},x} = \lambda_x \cdot T_{\text{norm}}$. For calculations, we will use $T_{\text{pulse}} = 1.4 \text{ ms}$, which is in agreement with the parameters used in [11].

2.3. Results

The explicit expressions derived in Section 2 describe the behavior of PSC transmission dependent on the modulation frequency. To evaluate these equations, we compare their resulting data with numerical simulations of the original iterative equations (2) and (3). Parameters for these simulations are identical to those used in Fig. 1, with the addition of $\lambda_1 = 130 \text{ s}^{-1}$ and $\lambda_2 = 6 \text{ s}^{-1}$. From these values, time constants τ_{u,λ_1} , etc. needed by the equations of Section 2 were calculated using the results of the appendix. For calculating the limit values u_{c,λ_1} , etc. and the initial values of a period in steady state, (5)–(6) and (10) with its counterparts were used, respectively.

Differing from the analytical equation, a sine-modulated Poisson process similar to the bursty spike train in the upper graph of Fig. 3 was used for the simulations instead of the deterministic square-modulated pulse train. Such a stochastic pulse train more closely resembles biologically realistic ones like the quasi-sine-modulated pulse train used in [8, Fig. 6]. Fig. 5 shows the behavior of PSC transmission.

For clarity, a logarithmic scale was used for the modulation frequency f_m . The simulation curve represents the averaged PSC over 30 sine-modulated Poisson pulse trains of length 2 s for each modulation frequency data point. Despite the different stimulation protocols and the continuous-time generalization of the time course of u and R used for the analytical expression, the two curves are in close agreement with each other. Both curves show only slight absolute variation in postsynaptic current, with the mean PSC being almost constant over a wide range of modulation frequencies.

Compared to the converged PSCs for constant high or low rate, 15.7 pA at 130 s^{-1} and 1.28 pA at 6 s^{-1} as derived from (5) and (6), the PSCs under modulation according to (13) calculate to 18.5 and 0.84 pA, thus being significantly higher on average. Note that the absolute PSC values of Fig. 5 also compare well with Fig. 3 of [13], where the product $u_n \cdot R_n$, when adjusted for spike

count, spike frequency and the synaptic efficacy A of [11], is equal to 10.4 pA.

Hence, the postsynaptic ‘efficiency’, i.e. the total current induced by a certain number of pulses, is increased for modulated or grouped pulse trains. Transmission of modulated pulse trains is therefore more efficient compared to constant rate pulse trains, which is in accordance with the experimental data [1,9].

In the simulation, this effect is present even for high modulation frequencies (f_m in the order of $1/\lambda_1$), since the progression from low to high modulation frequencies is similar to the biological one from bursting to stuttering to chattering [13], with chattering still being significantly different from a constant rate stimulus.² Therefore, u and R of the simulated iteration equations do not converge to steady-state values, but alternate between intermediate values. The relative variation of PSC with modulation frequency is due to the relatively high single pulse rates λ_1 and λ_2 , making the influence of the term for the increasing PSC in (2) relatively low [11]. The depression of the PSC is dominant, which is especially the case for low modulation frequencies, where R decreases significantly due to the time constant τ_{rec} . For high modulation frequencies this effect is not as strong as for low ones [1,7]. Therefore, the PSC increases with higher modulation frequencies, as can be seen from Fig. 5.

The dashed line in Fig. 5 shows the principal behavior for low λ_1 and λ_2 . In contrast to the high-rate case, the PSC decreases with higher modulation frequencies. Due to the lower single rates, τ_{facil} also has an influence on the behavior. For long modulation intervals, the slightly higher PSC response is governed by a fast depression with time constant τ_{rec} , followed by a facilitation with time constant τ_{facil} that increases the overall response. At higher modulation frequencies, the influence of τ_{facil} decreases, resulting in a lower PSC [13]. This effect can be observed in the analytical solution, as well as in simulations.

Fig. 6 shows the absolute time constants of u and R for two different parameter sets used in Fig. 5B of [13]. The corresponding optimal spike trains derived in [13] show marked transition between regular spiking with 20 Hz ($\tau_{\text{rec}} = 60 \text{ ms}$) and a burst mode with a burst pulse frequency of approx. 100 Hz and burst

² Interestingly, the optimal pulse trains in terms of PSC, as derived by the heuristic methods in [13] also run through these regimes and exhibit a very similar modulation. We will come back to this in Fig. 6.

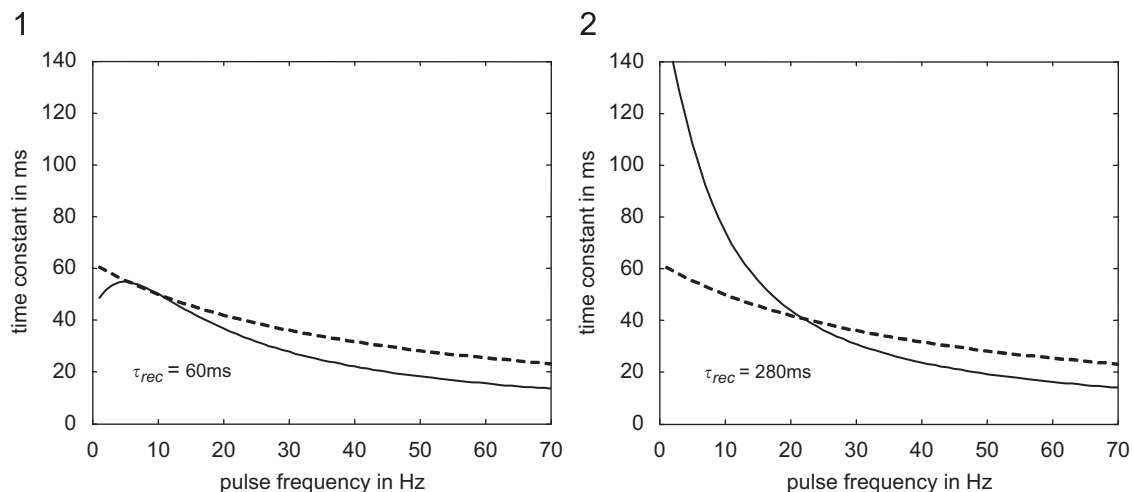


Fig. 6. Time constants $\tau_{u,\lambda}$ (dashed) and $\tau_{R,\lambda}$ (solid) with respect to pulse frequency λ for two parameter sets as used in Fig. 5B of [13] ($U = 0.32$, $\tau_{\text{facil}} = 62$ ms).

repetition rate of 8 Hz. When looking at the time constants of Fig. 6, the absolute time constants for u and R at $\tau_{\text{rec}} = 60$ ms are approximately equal for low pulse frequencies. Thus, to maximize $u \cdot R$ for a given total pulse number, they have to be distributed equally across the given time interval. This is due to the fact that u and R have opposing frequency dependence (see Fig. 2), but the same time constants, so to extract the maximum of the product $u \cdot R$, the slopes have to be sampled at regular intervals.

In contrast, for the second parameter value ($\tau_{\text{rec}} = 280$ ms), the time constant for R is significantly higher than the time constant for u at low pulse frequencies. Thus, R needs a longer time to recover between bursts (low frequency) than u , consequently a regime with very little to no pulses will increase the product $R \cdot u$, since its value mainly depends on R after u has already recovered due to its smaller time constant. On the other hand, the time constants for u and R at high frequencies are higher than the time between pulses in a burst (10 ms), so that adaptation to the high rate, especially the decay of R , will not have much influence on a burst of 2 or 3 pulses. Therefore, it is favorable for maximum transmission of a given number of pulses per unit time [13] to wait a longer time for recovery and then apply a short high-frequency burst which is too short for the synapse to adapt.

3. Conclusion

In extension of the work presented in [11,6,7,1], we have shown synaptic frequency selectivity of the quantal model not only for the pulse rate itself, but also for the modulation parameters, i.e. burst frequency, inter-burst-interval and burst duration. In [9], a similar, but simulation-based analysis has been carried out for a model of release probability. However, the complex dependence of synaptic transmission on the burst characteristics has been reported by [9] only for networks of several neurons and synapses, whereas our work shows this dependence for a single synapse employing quantal release plasticity.

A wide range of naturally occurring pulse trains could be subjected to detailed mathematical analysis using the model derived herein. For instance, the transient settling of u and R , which our analysis is based on (see appendix), can not only be observed for a modulation with two fixed pulse rates, but also for Poisson pulse trains, see Fig. 4 of [11]. Furthermore, as seen from Fig. 5, even with the approximations used in our

analytical model (fixed rate modulation, time-continuous synaptic dynamics) there is a very good correspondence with simulations employing the iterative quantal model and quasi-natural bursty spike trains. Thus, our analysis is also valid if the pulse rate during a burst is not constant. Accordingly, the general preferential treatment of bursts by dynamic synapses as derived in Section 2 could also be extended to cases where the information is contained in the fine structure of the bursts [9,7,12].

Also, the modulation does not have to be constant, i.e. pauses between bursts could vary, so that pulse trains derived in [12,13,15] could as well be treated with a more rigorous, global approach, rather than an analysis via simulations. In addition, the closed expression for the transfer function developed in this work could be employed to characterize the transfer/decoding function of synaptic networks, such as the ones used in [9].

Significant recent work in the neuroscience community tries to reinterpret this decoding function of neural networks with short-timescale-adapting synapses as an attractor network that switches to one of its states depending on external input and synaptical properties, thus modelling memory and decision making [16,1,3]. As shown for the limited example of Fig. 6, the preferences of synapses and thus the attractors of such a network (very likely some kind of repeating burst signal) could be analyzed more thoroughly based on our absolute time constants than on the original iterative ones.

Acknowledgments

The authors would like to gratefully acknowledge financial support by the European Union in the framework of the Information Society Technologies program, Biologically Inspired Information Systems branch, project FACETS (No. 15879).

Appendix A. Transient analytical description of quantal plasticity

The absolute convergence of iterative equations like those of the quantal model [11] is only defined for some special cases. The convergence limits for a constant presynaptic pulse rate λ can be derived with relatively little effort [11], but the speed of

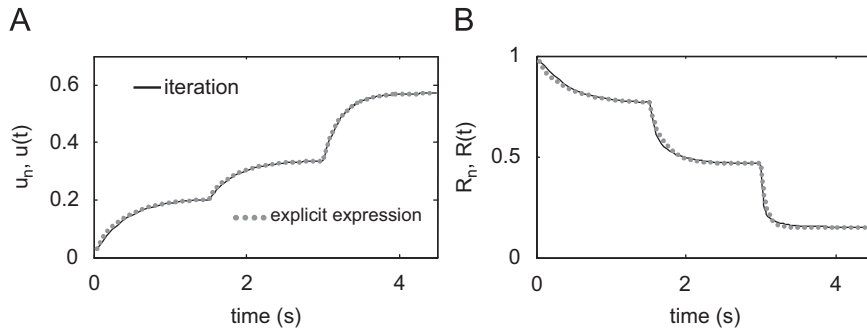


Fig. 7. Comparison of simulated and analytically derived time course of u (A) and R (B). Parameters are the same as used in Fig. 1.

convergence is difficult to define, especially due to the constant parts of the iterative equations for u_n , (2), and R_n , (3).

However, as Fig. 7 shows, in case of regular spike trains with a defined pulse rate, the iterative descriptions of u and R in (2) and (3) can be interpreted as settling of transient responses to a steady-state value, comparable to e.g. a resistance–capacitance voltage settling curve. In this case, an absolute time constant for this settling has to be derived, which is likely to depend on the fundamental time constants of the quantal model.

In the following, an explicit expression for the settling of u will be derived. Eq. (2), recursively describing the value of u after interspike interval (ISI) Δt_{n-1} , can be rewritten as

$$u_n = u_{n-1} \cdot e^{-\Delta t_{n-1}/\tau_{\text{facil}}} \cdot (1 - U) + U. \quad (14)$$

Note that all variables are shifted by one ISI compared to the original formulation. To be able to derive an explicit expression, we restrict ourselves to pulse trains having a constant rate λ , so that $\Delta t_n = 1/\lambda$ for all n . Recursively extending (14) by one ISI yields

$$u_n = u_{n-2} \cdot e^{-2/\lambda \cdot \tau_{\text{facil}}} \cdot (1 - U)^2 + U \cdot e^{-1/\lambda \cdot \tau_{\text{facil}}} \cdot (1 - U) + U. \quad (15)$$

The further recursion back to u_0 is obvious from (15). Together with the initial condition $u_0 = U$, this results in a sum over a geometric series:

$$u_n = U \cdot \sum_{i=0}^n (1 - U)^i e^{-i/\lambda \cdot \tau_{\text{facil}}} = U \cdot \sum_{i=0}^n [(1 - U)e^{-1/\lambda \cdot \tau_{\text{facil}}}]^i. \quad (16)$$

Because the term $(1 - U)e^{-1/\lambda \cdot \tau_{\text{facil}}}$ never exceeds the interval $[0,1]$, this series converges, and its sum can be calculated as [5]

$$u_n = U \frac{[(1 - U)e^{-1/\lambda \cdot \tau_{\text{facil}}}]^{n+1} - 1}{(1 - U)e^{-1/\lambda \cdot \tau_{\text{facil}}} - 1}. \quad (17)$$

The limit for $n \rightarrow \infty$ is the same as the value for $u_c(\lambda)$ calculated in (5). For the remainder of this derivation, it is convenient to write (17) in the following form:

$$u_n = \left(U - \frac{U}{1 - (1 - U)e^{-1/\lambda \cdot \tau_{\text{facil}}}} \right) \cdot ((1 - U)e^{-1/\lambda \cdot \tau_{\text{facil}}})^n + \frac{U}{1 - (1 - U)e^{-1/\lambda \cdot \tau_{\text{facil}}}}. \quad (18)$$

The speed of convergence is determined by the term dependent on n . Using the equality $n = \lambda \cdot t$, which is a generalization of the assumption $\lambda = 1/\Delta t_n$, this term gets:

$$((1 - U)e^{-1/\lambda \cdot \tau_{\text{facil}}})^{\lambda \cdot t} = e^{t \cdot [\lambda \cdot \ln(1 - U) - 1/\tau_{\text{facil}}]} = e^{-t/\tau_{u,\lambda}}, \quad (19)$$

with the time constant $\tau_{u,\lambda}$ describing the speed of convergence:

$$\tau_{u,\lambda} = \frac{1}{\lambda \cdot \ln\left(\frac{1}{1 - U}\right) + \frac{1}{\tau_{\text{facil}}}}. \quad (20)$$

The time constant thus is dependent on both the time constant of the iteration, τ_{facil} , and the pulse rate, λ . Therefore, (18) can be modelled as follows:

$$u(t) = (u_0 - u_c)e^{-t/\tau_{u,\lambda}} + u_c. \quad (21)$$

An explicit expression for R_n can be derived in a similar way, starting with an equation analogous to (15). Eq. (21) and its counterpart for R_n were verified against simulations of the iteration formulae (2), (3) over a wide range of parameters τ_{facil} , τ_{rec} and U , with good results. Fig. 7 shows an example. The differences between simulated and analytically derived $u(t)$ and $R(t)$ are due to the discrete nature of the original, iterative equations that were generalized to continuous time for the analytical formulation.

References

- [1] L. Abbott, G. Wade, W. Regehr, Synaptic computation, *Nature* 431 (14) (2004) 796–803.
- [2] P. Aguiar, D. Willshaw, Hippocampal mossy fibre boutons as dynamical synapses, *Neurocomputing* 58–60 (2004) 699–703.
- [3] O. Barak, M. Tsodyks, Persistent activity in neural networks with dynamic synapses, *PLoS Computational Biology* 3 (2) (2007) 323–332.
- [4] C. Bartolozzi, G. Indiveri, Selective attention implemented with dynamic synapses and integrate-and-fire neurons, *Neurocomputing* 69 (2006) 1971–1976.
- [5] I. Bronshtein, K. Semendyayev, G. Musiol, H. Muehlig, *Handbook of Mathematics*, Springer, Berlin, 1997.
- [6] A. Farajidavar, S. Saeb, K. Behbehani, Incorporating synaptic-time-dependent plasticity and dynamic synapse into a computational model of wind-up, *Neural Networks* 21 (2–3) (2008) 241–249.
- [7] G. Fuhrmann, I. Segev, M. Markram, H. Tsodyks, Coding of temporal information by activity-dependent synapses, *Journal of Neurophysiology* 87 (2002) 140–148.
- [8] F. Gabbiani, W. Metzner, Encoding and processing of sensory information in neuronal spike trains, *The Journal of Experimental Biology* 202 (10) (1999) 1267–1279.
- [9] J. Jenca, J. Pavlásek, Some implications of the short-term synaptic plasticity for neuronal computation: a model study, *Biologia, Section Cellular and Molecular Biology* 62 (4) (2007) 498–506.
- [10] C. Koch, *Biophysics of Computation: Information Processing in Single Neurons*, Oxford University Press, USA, 2004.
- [11] H. Markram, Y. Wang, M. Tsodyks, Differential signaling via the same axon of neocortical pyramidal neurons, *Proceedings of the National Academy of Sciences of the USA* 95 (1998).
- [12] V. Matveev, X.-J. Wang, Differential short-term synaptic plasticity and transmission of complex spike trains: to depress or to facilitate?, *Cerebral Cortex* 10 (2000) 1143–1153.
- [13] T. Natschläger, W. Maass, Computing the optimally fitted spike train for a synapse, *Neural Computation* 13 (2001) 2477–2494.
- [14] E. Persi, D. Horn, R. Segev, E. Ben-Jacob, V. Volman, Neural modeling of synchronized bursting events, *Neurocomputing* 58–60 (2004) 179–184.
- [15] B. Sengupta, D. Halliday, Neuronal dynamics of dynamic synapses, in: *Proceedings of the 27th IEEE Annual Conference on Engineering in Medicine and Biology*, 2005.
- [16] J. Torres, J. Cortes, J. Marro, H. Kappen, Competition between synaptic depression and facilitation in attractor neural networks, *Neural Computation* 19 (2007) 2739–2755.



Christian Mayr received the Dipl.-Ing. (M.Sc.) in Electrical Engineering in 2003 and his Ph.D. in 'Implementations of image processing in pulse-coupled neural networks' in 2008, both from the University of Technology Dresden, Germany. Since 2004, he has been a research assistant with the Chair for Parallel VLSI-Systems and Neural Circuits at the TU Dresden. His research interests include bio-inspired circuits in general, information processing in spiking neural nets in both simulation and hardware, and mixed-signal VLSI-design. He is author or co-author of over 20 publications in the subject areas mentioned above and has acted as reviewer for IEEE TCAS & TNN journals, Elsevier journals, MWSCAS and NIPS Conferences.



Rene Schüffny received the Dr.-Ing (Ph.D.) and the Dr.-Ing. habil. (D.Sc.) degrees from the University of Technology Dresden, Dresden, Germany, in 1976 and 1983, respectively.

Since April 1997, he has held the endowed chair for massively parallel VLSI systems and neural circuits at the University of Technology Dresden. His research interests include CMOS image sensors and vision chips, design and modelling of analog and digital parallel VLSI architectures, and neural networks. He is author or co-author of numerous publications in the above field and has acted as reviewer for several international journals.



Johannes Partzsch obtained his M.Sc. in Electrical Engineering from the University of Technology Dresden, Germany in 2006. He is currently working on his Ph.D. in 'Optimized architectures for large-scale neuromorphic circuits' at the Chair for Parallel VLSI-Systems and Neural Circuits, TU Dresden, Germany. His research interests include bio-inspired circuits, topological analysis of neural networks and modelling of synaptic plasticity.